15th International Symposium on Flow Visualization - ISFV15
June 25-28, 2012, Minsk, Belarus

Experimental and computational analysis of the flow induced by a piezoelectric fan

M. Ahmadi Bidakhvidi[1], S. Vanlanduit, R. Shirzadeh, D. Vucinic

[1]Department of Mechanical Engineering, Vrije Universiteit Brussel, Brussels, Belgium
mahmadib@vub.ac.be

ABSTRACT

The use of piezoelectric ceramics as actuators in flapping plate systems is interesting due to the low power consumption and high energy efficiency. Fluid flow is induced by these piezoelectric fans by converting electric energy into mechanical vibrations with the use of piezoelectric patches bonded to a passive elastic plate. By applying an alternating voltage the patch will periodically start to contract and expand. If the frequency of the AC voltage is equal to the first resonance frequency of the structure, a sufficiently large dynamic tip deflection can be obtained, which is required to induce an air flow by the flapping plate. A considerable increase in heat transfer could be obtained by using these piezo fans for cooling of electronic devices [2]. Another application is applying these piezoelectric oscillating mechanical systems as flapping wings for MAVs [6]. The motion of the piezo fan is determined by the actuation frequency and the modal parameters. The structural optimization of these systems, in terms of optimizing the tip deflection and efficiency, does not necessarily match the optimization of the flow induced by the oscillating wing. This flow is characterized by a coupled fluid-structure interaction. A 2D assumption was made in many past studies found in the literature. However the flow behind wings with finite span is significantly more complex than the flow behind infinite span wings. In this present study experimental high speed PIV measurements are conducted on a piezoelectric flapping wing with finite span operating at 84.8 Hz in air. The structure was operated at different tip deflection amplitudes, controlled by an integrated Laser Doppler Vibrometer system in the experimental set-up. The time resolved and RMS time-averaged results for different amplitudes are compared to 2D and 3D LES CFD simulations as a validation of the numerical method. Dominant Proper Orthogonal Decomposition (POD) modes were determined to obtain the dominant flow characteristics.

1. INTRODUCTION

The use of piezoelectric ceramics as actuators in flapping plate systems is very interesting due to the low power consumption and high energy efficiency. Fluid flow is induced in these systems by converting electric energy into mechanical vibrations with the use of piezoelectric patches bonded to a passive elastic plate. By applying an alternating voltage the patch will periodically start to contract and expand (Fig. 1). If the frequency of the AC voltage is equal to the first resonance frequency of the structure, a sufficiently large dynamic tip deflection can be obtained, which is required to induce an air flow by the flapping plate. It has been shown that this flow can provide enhancements in heat transfer with minimal power requirements.

The first effort on piezo fan flow simulations has been reported in [1] where simplified models of the air flow and vibration were discussed with attention to the possible applications. A considerable increase in heat transfer could be obtained by using these piezo fans for cooling of electronic devices [2]. They discovered that piezo fans exhibit significant advantages over conventional axial fans by requiring less power. A clear miniaturization trend can be observed for electronic devices, making the development of smaller cooling piezo fans essential, since piezoelectric actuators can be scaled down easily. A closed-form analytical solution of the dynamic response of a resonant, composite piezoelectric beam was developed for the optimization of piezo fans. This model allowed the prediction of the optimal patch-to-beam ratio, patch location and patch-to-beam thickness depending on whether the the efficiency (EMCF), tip deflection or frequency was posed as optimization criterion [3].

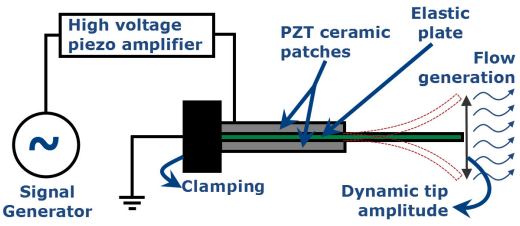

Figure 1: The principle of an operating piezoelectric flapping plate

The need to understand the basic principles of flapping flight increases since the mimicking of natural fliers is important in the design of Micro Aerial Vehicles (MAVs). Another application is applying these piezoelectric oscillating mechanical systems as flapping wings for MAVs. It is demonstrated by flying insects and birds that flapping flight is advantageous for its superior maneuverability and lifting capability at very low Reynolds numbers. There have been several studies in recent years to explore the potential application of piezoelectrically actuated flapping plates as compact flapping wings for MAV designs [4] [5] [6].

A 2D CFD beam model of a piezoelectric fan displacement was used in [7]. They described the first mode shape (resonance frequency of 60 Hz) of a commercial piezoelectric fan with an equation dependant on the dimensions/material properties. Using the equation for beam location during vibration, a user-defined function was called in Fluent to provide the boundary along the beam. The equation was set up for 60 Hz. Variation of heater plate proximity and fan deflection amplitude were considered through a design of experiment approach and compared to available experimental data. Four regions of circulation could be seen in the velocity plots presented when the heater plate was close to the fan tip. Due to proximity to the object, fluid velocities were relatively larger in magnitude than the other cases with larger beam to plate distances.

Recently a few studies focused on the experimental flow characterization of these flows. In [8] an experimental investigation was conducted to characterize the evolution of

the unsteady vortex structures in the wake of a root-fixed piezoelectric flapping wing. A PIV system was used to achieve phase-locked measurement to quantify the transient behavior of the unsteady wake vortex structures in relation to the phase angles of the piezoelectric flapping wing in the flapping motion. A wavelet-based vortex analysis and the Proper Orthogonal Decomposition (POD) method was used in [9] to show the characteristics induced by a vibrating cantilever plate. The results showed clearly that the investigation of phase-averaged data hides several key flow features. Careful data post-processing is therefore necessary to investigate these highly transient periodic flows.

In the present study, an experimental investigation was conducted to quantify the unsteady aerodynamic characteristics of a piezoelectric flapping plate to be able to compare to the 2D and 3D computational results.

2. EXPERIMENTS

2.1 LDV experiment

Important geometrical and physical parameters of the piezoelectric flapping plate used in both the numerical and experimental setups in this work are given in Table 1. The dynamic tip deflection is defined as the peak-to-peak maximum deflection given at the first bending mode when a voltage of 120V AC is applied on the piezoelectric patches. For the experiments a bimorph actuated piezoelectric flapping plate was used [10].

Properties	
Total Length	62.5 mm
Thickness Elastic Plate	0.4 mm
Thickness Piezo Patch	0.25 mm
Width	11.6 mm
First Resonance Frequency	84.84 Hz
Dynamic Tip Amplitude	10.3 mm
Weight	3.76 gram

Table 1: Geometrical and physical parameters of the piezoelectric flapping plate.

The mode shapes and resonance frequencies of the flapping plate were determined experimentally by measurements using scanning laser Doppler vibrometry (LDV) analyzer (PSV-400). These dynamic properties of the structure were also used in the numerical modeling of the flapping plate.

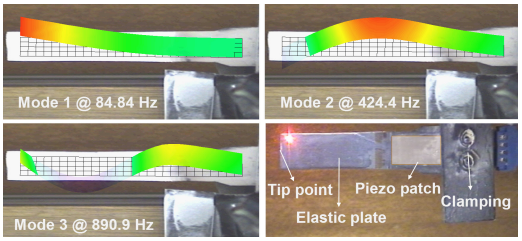

Figure 2: Mode shapes of the flapping plate structure.

The tip deflection is an important parameter for the induced flow field by the flapping motion. This will also be confirmed by the PIV experiments in Section 2.2. The measured relationship between the applied AC voltage and tip displacement is given in Fig. 3).

From the experiments a 6th-order polynomial fit is used to represent the first mode shape with a peak-to-peak deflection

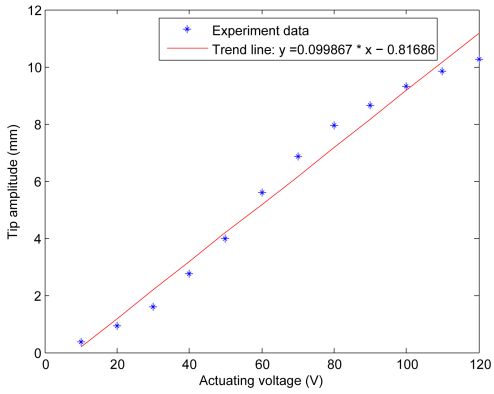

Figure 3: Flapping amplitude versus applied AC voltage.

of 10.3 mm:

$$f(x) = (-212334.25x^6 + 54750.2x^5 - 4496.08x^4 + 137.62x^3 + 0.71x^2 - 0.0086x + 9.61 \cdot 10^{-6}) \cdot sin(2\pi ft) \quad (1)$$

In Eq. 1 the flapping motion is described in function of the time t; x is the coordinate of the flapping plate in meters; f is the frequency of the applied voltage on the piezo patches, consequently the flapping frequency of the plate.

2.2 PIV experiment

The experiments were conducted in a closed domain with optically transparent walls and with dimensions 0.5 m long x 0.25 m wide x 0.3 m high. The piezoelectric flapping plate was clamped on a stiff base and placed in the center of the enclosure to reduce the effects of the domain walls near the tip of the flapping plate, which is the main region of interest for the PIV measurements.

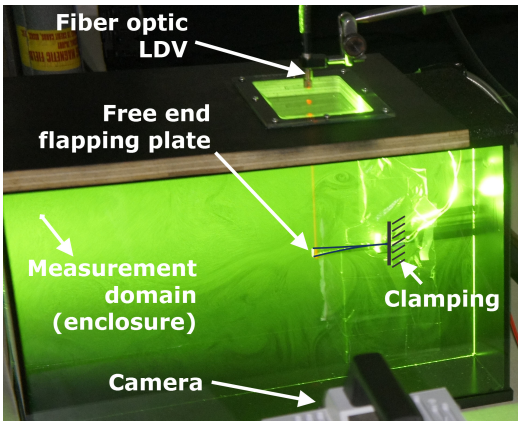

Figure 4: Clamped piezoelectric flapping plate in the enclosure with integrated LDV system.

The boundary walls could have a strong influence on the flow structures induced by the flapping motion of the plate. The stiffness of the clamping has a significant influence on the performance of the flapping system [11] and should be as stiff as possible. The electronic wiring of the piezoelectric device were housed in the clamping base. A LDV system (Polytec OFV 501) was integrated in the PIV flow measurement set-up to be able to check the resonance frequency and tip deflection (Fig. 4).

Illumination was provided by a double pulsed Nd:YLF laser (Quantronix Darwin Duo: 527 nm wavelength, 2 x 32

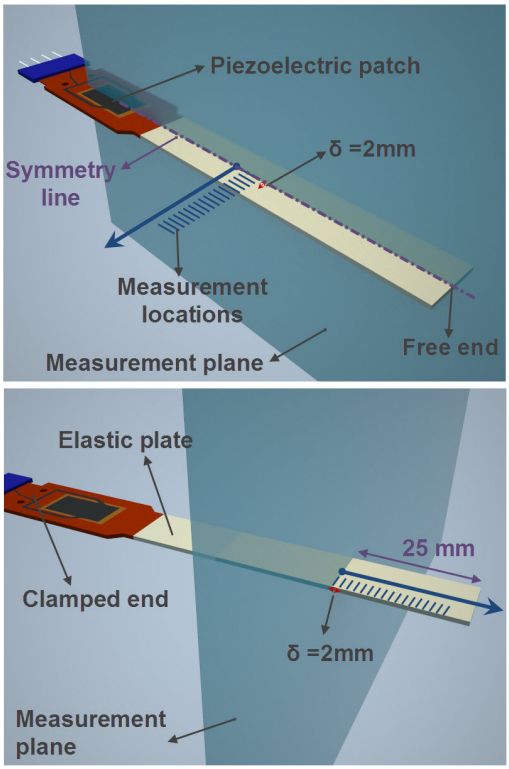

Figure 5: The defined PIV measurement planes on the piezoelectric flapping plate. Top: planes parallel to the plate (series 1). Bottom: planes perpendicular to the plate (series 2).

mJ/pulse). The thickness of the laser sheet is estimated to be about 1 mm. Images of the flow field were taken by a high speed CMOS camera (Photron SA1.1). The laser and the camera were connected to a computer via a synchronizer with a resolution of 5 ns (ILA Synchronizer) that controlled the timing of the laser pulse and image acquisition. The experiments were carried out in an air-conditioned room to avoid significant temperature rise because of the heat generation of the high power laser. Seeding particles with diameters between $1-5$ μm were injected in the domain using a fog generator which heated up N_2 gas. This was done by a tube placed behind the clamp base to minimize the effects of the introduced seeded flow on the flow induced by the oscillating plate at the tip. The particles were homogeneously distributed over the domain and had a diameter of 2-3 pixels in the recorded images.

A sinusoidal signal from the function generator (Agilent 33220A) was supplied to the linear amplifier (Piezo Systems EPA-104) where it was amplified to 120 Volt. This voltage was applied on the piezoelectric patches of the flapping wing to drive the oscillating motion. The Reynolds numbers based on the wing tip velocity was calculated using Eq. 2, where U_{tip} is the maximum velocity of the tip, c is the span width of the plate, a is the peak-to-peak amplitude and ν is the dynamic viscosity of air. For our test case a Re of 5383 was obtained.

$$Re = \frac{U_{tip} \cdot c}{\nu} = \frac{(2\pi a f)c}{\nu} \tag{2}$$

The high speed PIV analysis was conducted on a set of 2000 frames obtained at a speed of 4000 frames per second using the high speed camera. Each image captured by the camera has a dimension of 1024 x 1024 pixels. From the obtained PIV images for every time step $\Delta t = 250$ μs an instantaneous PIV velocity vector field was obtained by applying a frame to

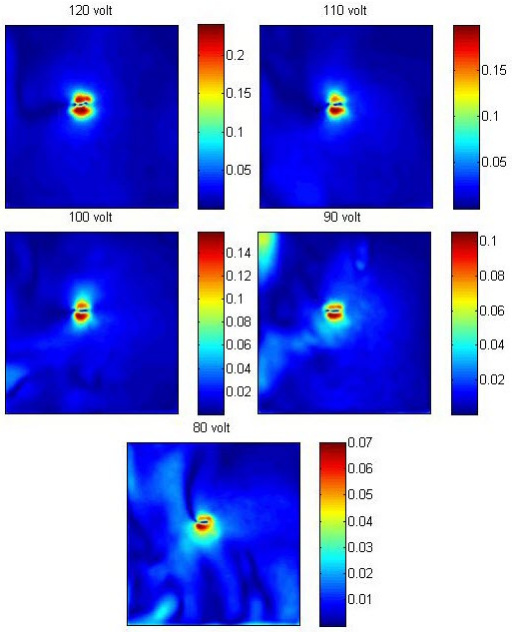

Figure 6: Time-averaged contour plots obtained from experiments measured in in the cutting plane at a distance of 25 mm from the tip ($\delta = 0$) and perpendicular to the symmetry plane for different voltages resulting in different peak-to-peak tip deflections of the flapping plate.

frame cross correlation technique on the different interrogation windows. An adaptive multiple grid interrogation algorithm was employed where the initial coarse grid is refined to a final fine grid [12]. The initial interrogation window size was 96 x 96 pixels and the final window size 8 x 8 pixels with 50% overlap. Outliers were removed using a median filter with dynamic threshold. A sub-pixel image shifting was enabled on all passes.

Measurements were conducted on different positions parallel to the oscillating plate (series 1) and perpendicular to the plate (series 2), as given in Fig. 5. For every new measurement the laser sheet was shifted 2 mm away from the previous measurement plane. This distance is accumulated in δ, which is dependant on the initial measurement plane.

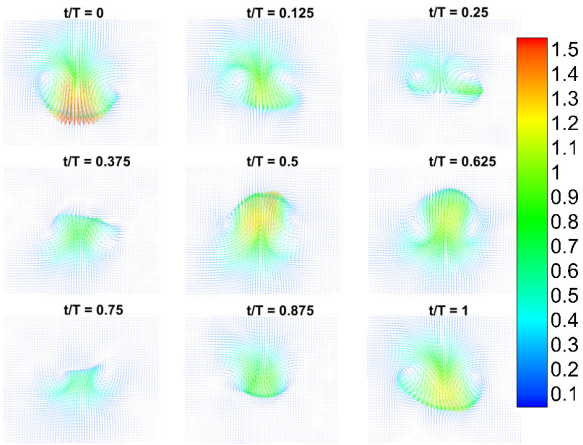

Figure 7: Instantaneous vector field plots of the flapping plate obtained from experiments measured in the plane perpendicular to the plate ($\delta = 4mm$) for different time steps over one period T.

The initial measurement plane for series 1 (i.e. parallel to the flapping plate) is defined as the plane cutting the plate in half along the length on the symmetry line (Fig. 5). Because of the symmetry, measurements were done for δ from 0 to 36 mm in one direction away from the initial plane. The initial measurement plane for series 2 (i.e. perpendicular to the plate) cuts the flapping plate 25 mm from the tip (Fig. 5). Measurements were done for δ from 0 to 32 mm. The location of the laser sheet relative to the flapping plate for the different measurements was controlled by a highly accurate traversing system with DC motors to guarantee repeatability of the experiments. The laser beam was shaped to a sheet by a set of mirrors through an articulated mirror arm system to spherical and cylindrical lenses.

Fig. 8 shows the velocity vectors for series 1 ($\delta = 0$). The vectors are obtained for measurements at different times when the fan swings downward and upward, completing one oscillation period or T = 1/84.84 Hz = 0.0118 s. These results show that the induced flow by a piezoelectric flapping plate is an unsteady phenomenon: the velocity vector field induced is very much dependent on the fan position in the period (t/T). At $t/T = 0$ the plate is at its neutral position moving downwards. A vector field is shown from the previous period. The maximum velocity appears slightly before the tip of the plate. A vortex is being shed when the flapping plate has already made an upward sweep and is heading back down towards the lower extreme position. This clockwise moving vortex continues to get developed and moves towards the upper part of the flapping plate tip at $t/T = 0.083$ and $t/T = 0.167$. The velocity increases when the plate reaches its lower extreme position, causing the vortex to break out ($t/T = 0.25$). The velocity near the tip builds up again when the plate moves upward towards the neutral position shedding a new vortex at $t/T = 0.5$. This counter-clockwise moving vortex continues to get developed further until the plate reaches it extreme upper position. Due to the downwards motion the velocity decreases and the vortex breaks out at $t/T = 0.833$, while later a new clockwise moving vortex is shed when the plate moves to the neutral position ($t/T = 1$). This flow phenomenon keeps repeating itself for every period. The mean velocity vector field is also given in Fig. 8 showing a high velocity region near the tip followed by a low velocity region due to the vortex shedding. Two jets moving away from the fan can be observed. First the fluid is pulled into a small area by the flapping plate just before the tip end with high velocities, then it is pushed away over a larger area because of the vortex shedding phenomenon, which is manifested in two jets in the mean flow field. The background image from the PIV analysis is also given in Fig. 8 so that the motion of the plate easily could be followed for the different time steps in one oscillation period. Also the seeding particles are visible.

Fig. 7 shows the evolution of the flow phenomenon around the flapping plate at different selected instances for series 2 ($\delta = 4mm$). For almost every presented time steps in a period T the vortex structures can be observed and tracked. The unsteady flow measured in series 2 is characterized by double vortices which are generated twice in one oscillation of the plate. When the plate swings downward and upward it creates a counter-rotating vortex pair with high velocities located between the vortices. The vortex pairs are connected to each other at the tip of the plate following the edges of the plate. At $t/T = 0$ the plate is at the neutral position and moving downwards towards the lower extreme position. The velocities decrease when the lower extreme position is reached. When the plate is moving back upwards the vortices break out and new vortices are formed ($t/T = 0.375$). This pair gets stronger and the velocity increases to reach a maximum when the plate is near the neutral position ($t/T = 0.5$). The same flow phenomenon occurs when the plate moves back upward to the higher extreme position to slow down and move backwards again to the neutral position, completing the oscillation ($t/T = 1$).

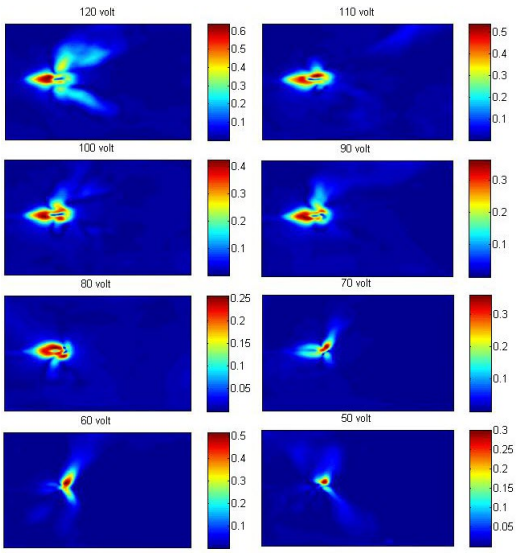

Figure 9: Time-averaged contour plots obtained from experiments measured in in the symmetry plane ($\delta = 0$) for different voltages resulting in different peak-to-peak tip deflections of the flapping plate.

Mean velocity contours are given for series 1 measurements in Fig. 10. The edge of the plate is at 5.8 mm from $\delta = 0$ plane, thus for $\delta > 6mm$ the laser sheet did not cut the flapping plate. For low δ values the mean velocity field is characterized by a high velocity area just before the tip end, followed by a sudden low velocity area representing the vortices generated in upward and downward direction for every oscillation of the plate. Two jets can be observed moving away from the plate with low mean velocities. For higher δ these jets get dominant and diverge.

The mean velocity field of the beam cross-section (series 2) has a distinct shape. These results for different δ are given in Fig. 11. For low delta values $\delta = 0 - 8mm$ two peak velocity zones are detected representing the periodic vortex pair generation in upward and downward direction. Between these zones there is a low velocity zone because the velocity is averaged out to 0 because of the harmonic motion. For higher δ this zone will have a larger area because the tip motion increases and four jets can be observed moving away from the plate. These jets provide a constant flow of the fluid but have low velocities.

Decreasing the flapping amplitude reduces the speed of the tip of the plate. This was obtained by reducing the applied voltage. The mean velocity contour plots for series 1 show that the flow phenomenon is highly dependent on the amplitude of the plate for the same frequency. Therefore the mean velocity of the flow does not necessarily increase with higher voltages. The relationship between the applied voltage on the piezo patches and the induced dynamic tip deflection of the elastic plate is given in Fig. 3. For the results of 50 and 60 Volt there is an increase of the mean velocity of the two jets pointing away from the tip of the flapping plate (Fig. 9). The tip vortices are too small to be observed accurately by the measurement. At 70 Volt there is a transformation of the flow to a flow type characterized by the higher amplitudes. The vortices for increasing amplitudes do get observed, expressing itself as low

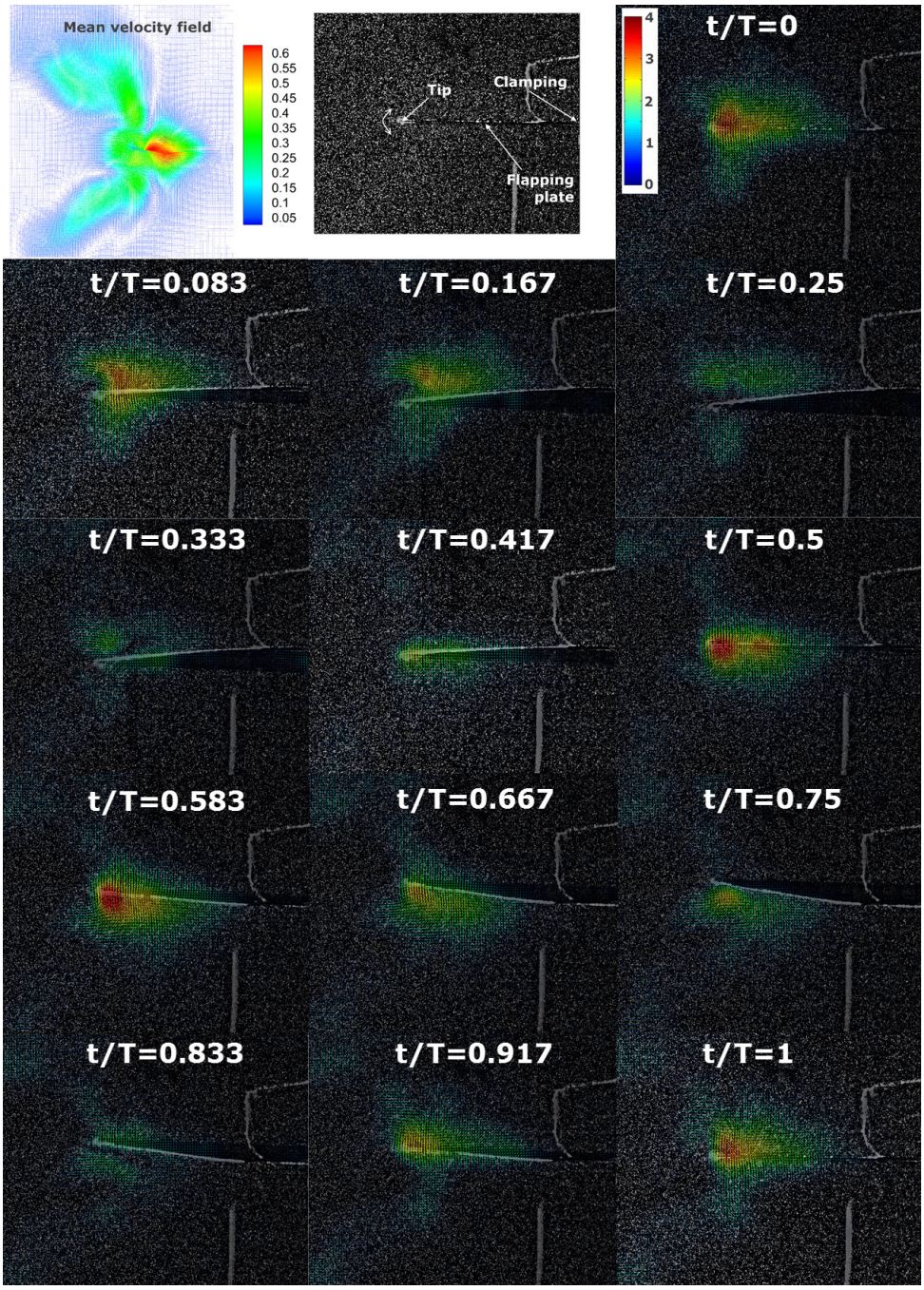

Figure 8: Instantaneous vector field plots of the flapping plate obtained from experiments measured in the symmetry plane (δ=0) for different time steps over one period T. The top left image gives the time averaged vector field over multiple periods.

velocity zones surrounded by high velocity zones for the mean flow (Fig. 9).

The mean velocity contour plots at the beam cross section (series 2) show that the flow phenomenon does not change for different amplitudes such as the results for series 1. The mean velocities increase with increasing amplitude (Fig. 6) due to the increase of the plate velocity.

3. COMPUTATIONAL STUDY

Although the flapping plate was actuated by piezoceramic patches attached to the plate, the geometry in the numerical model is reduced to that of a beam without the presence of the piezoelectric patches. The thickness of the patches in the model is negligible. The presence of the clamp holding the piezoelectric flapping plate is assumed to affect the flow field, however this is not taken into account in the numerical model. The region of interest from the numerical results is located near the tip of the flapping plate.

For the numerical simulations the commercially available computational fluid dynamics software package ANSYS CFX is used. A second order accurate central difference advection scheme was used. A second order backward Euler scheme was used for the time discretization. At every new physical time step the deformed mesh has to be calculated. The control

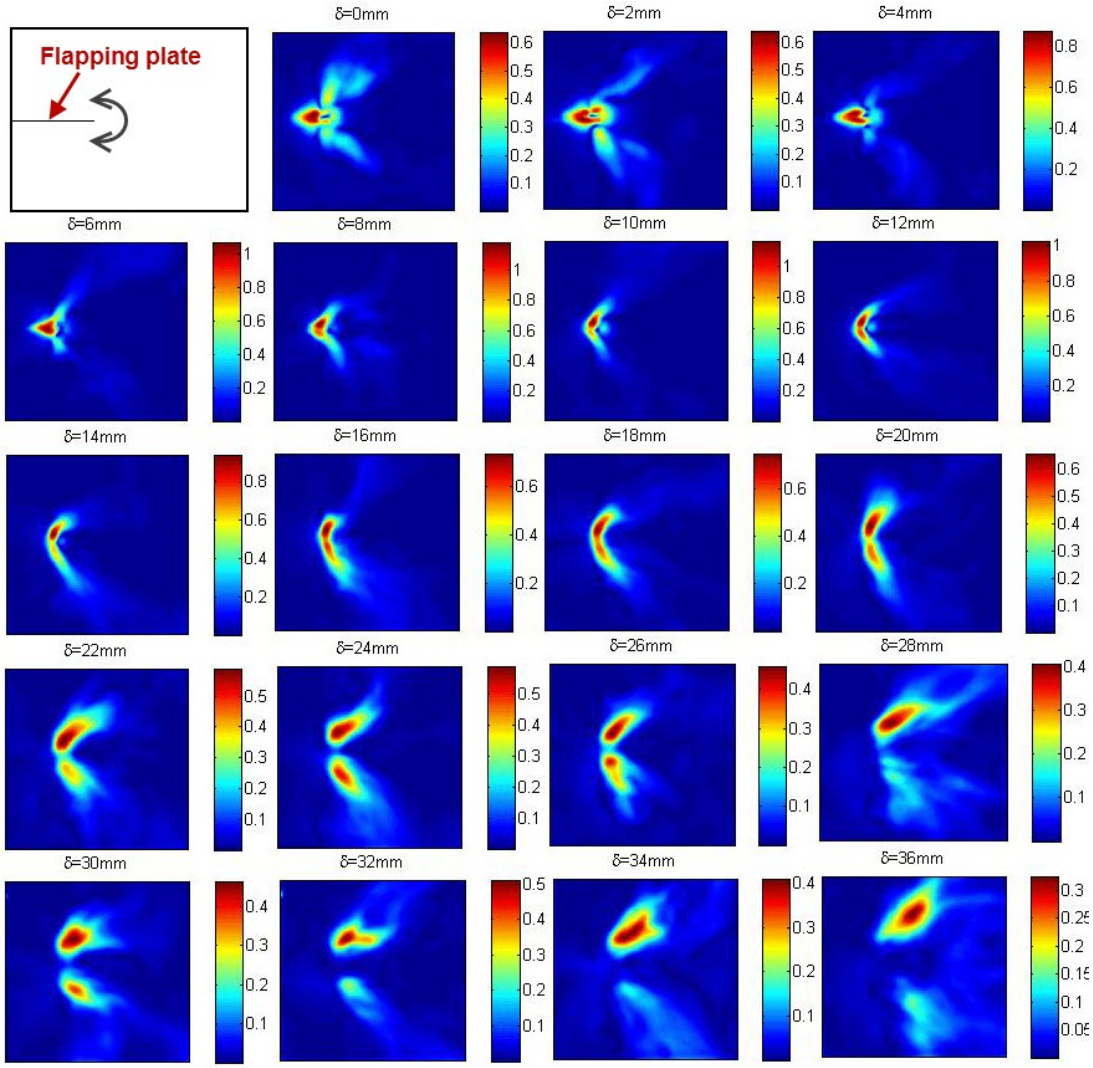

Figure 10: Time-averaged contour plots of the flapping plate obtained from experiments measured in different planes parallel to the symmetry plane ($\delta = 0$ to $36mm$).

volumes are subjected to translation or deformation and the Navier-Stokes equations have to be extended by a term, which describes the relative motion of the surface element with respect to the fixed coordinate system. Such deformations are handled without remeshing. If the mesh movement is too large over time it can lead to poor quality meshes and even negative mesh volumes. It was necessary to increase the mesh stiffness near small volumes for the models to avoid folding of the mesh in the regions where the displacement was large. The fluid is defined as air which we can consider as an incompressible flow in our case, because only low velocities are induced by the flapping plate. Also there is no region where the pressure can keep building up. The density and dynamic viscosity used in the numerical calculations are given as $1.185 \frac{kg}{m^3}$ and $1.831 \cdot 10^{-5} \frac{kg}{m \cdot s}$.

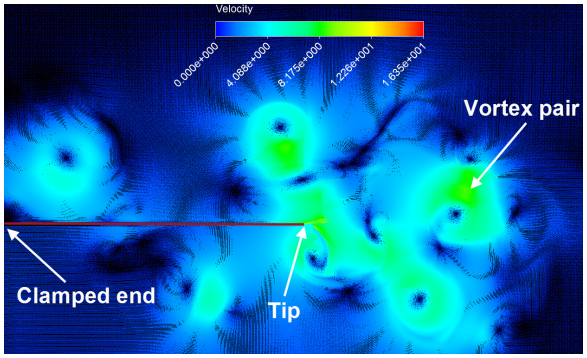

Figure 12: The 2D LES vector field for $t/T = 10$.

The Large Eddy Simulation (LES) model was used as turbulence model for the unsteady flow. The flow variables are decomposed into large and small scale parts. LES solves for large scale fluctuating motions and uses sub-grid scale turbulence models for the small scale motion. The flow is dominated by large-scale vortices shed from the oscillating body. There is a strong interaction between the vortices, letting them break apart, and provide intensive mixing that is not produced by any turbulence models (e.g. Spalart-Allmaras, k-ε, k-ω) in Reynolds-averaged Navier-Stokes equations (RANS). It is generally known that RANS models fail to predict such complex flows with a proper accuracy. So it is important to apply some of the vortex resolving turbulence models, like Direct Numerical Simulation (DNS), LES or a RANS-LES

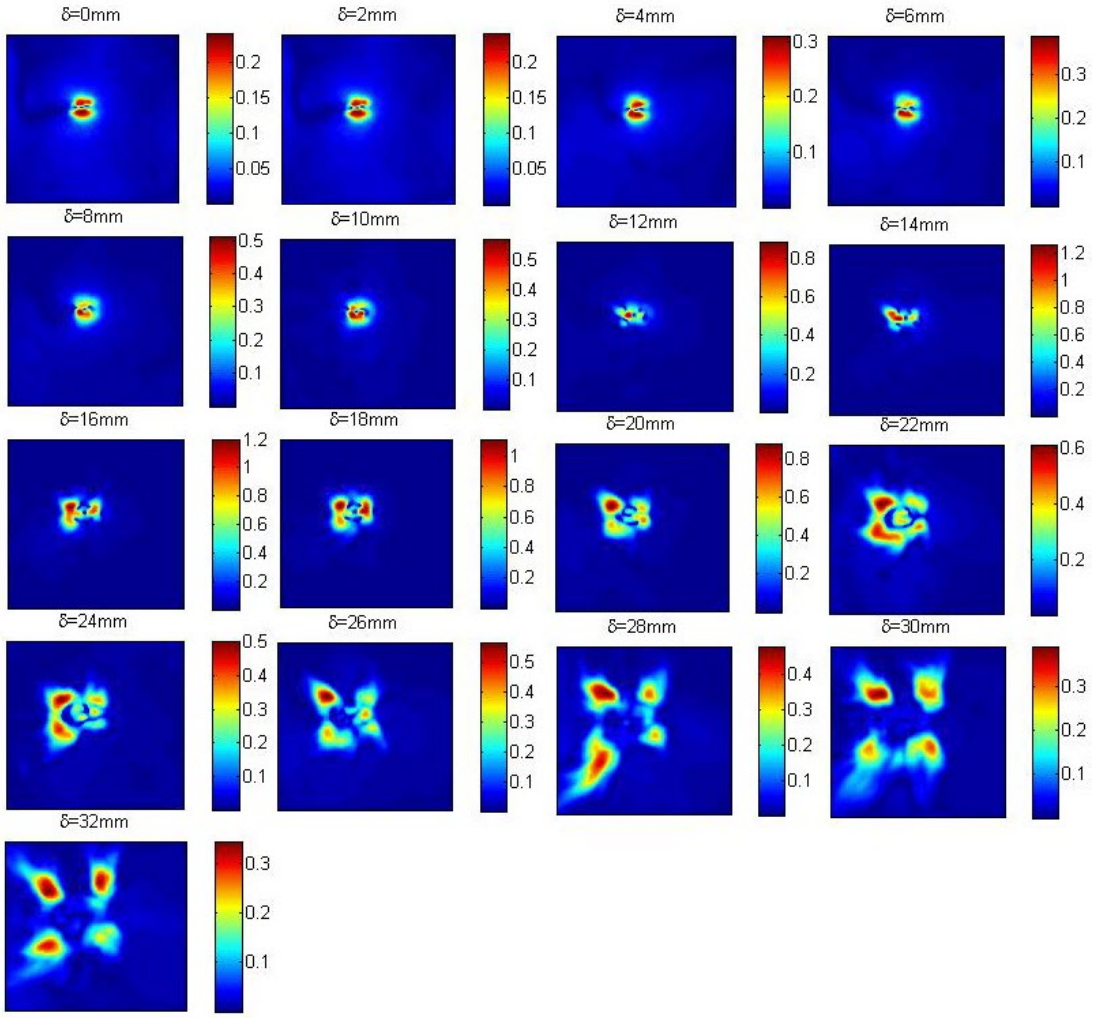

Figure 11: Time-averaged contour plots obtained from experiments measured in different planes perpendicular to the symmetry plane cutting the flapping plate ($\delta = 0$ to $32mm$).

hybrid. Due to the huge calculation cost of DNS, in this present work LES is applied.

In order to capture the flow field correctly a proper time step is required. A time step of $25 \cdot 10^{-6}$ s was chosen for the numerical simulations, which means more that 471 steps were calculated per oscillation period of the flapping plate. The oscillations are forced by a prescribed harmonic motion computed from the LDV measurements (Eq. 1). The moving flapping plate is defined as a no slip wall boundary, while the other boundaries are defined as openings. The opening boundary condition is used because the pressure is known, but the direction of the flow is unknown at the outer boundaries. This allows flow entering and leaving the fluid domain.

Both 2D and 3D simulations were conducted for this test case. The flapping plate vibrated at the first bending mode with a tip deflection of 10.3 mm, as determined with the experiments in Section 2.1. The computational grid for the 2D and 3D case consisted of 1.5 and 15 million elements, respectively. The 3D domain size is 0.14 m long x 0.08 m wide x 0.15 m high. A mirror symmetry condition at the middle plane is defined for the 2D simulation case. To be able to compare the computational and experimental results for the 3D case, different 2D planes in the computational domain have to be defined. Therefore the calculated quantities have to be interpolated on the planes. Vector quantities need to be projected on the user defined planes to obtain a 2D vector field from the 3D results. The 2D mean velocity field has been extracted out of the 3D numerical results for the symmetry plane and beam-cross section 25 mm away from the tip in Fig. 14. The computations were carried out on 12 processors (2.8 GHz).

The vector field from the 2D numerical calculations (Fig. 12) is rather chaotic and contains many vortices that do not break out easily in time in contrast to the 3D numerical results. The flow is characterized by a large amount of vortex pairs, these are two counter-rotating vortices whose induced velocities tend to augment a momentum. If the two vortices have the same circulation of magnitude, but an opposite sense of rotation, then the velocity of each vortex at the location of the other is directed in the same sense. The entire system therefore translates at a speed relative to the fluid. These vortices will continue to move under the action of the velocity induced by the other vortex and do not remain stationary. For every oscillation of the plate, two vortices are shed which form a vortex pair. These vortex pairs interact with other pairs resulting in a chaotic flow character. When the wing keeps oscillating more vortices can be observed. These vortices continue to emerge and move away from the point of origin, while being combined with other vortices. A plate with a large width would be required to be able to match the 2D numerical model, so that its mid-plane would be largely

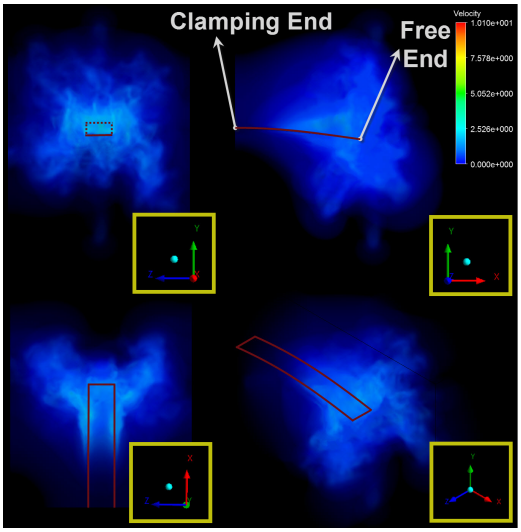

Figure 13: Volume rendering by variable transparency of the velocity contour plots in function of the velocity value obtained from 3D computational model.

2D in behavior, with minimal edge effects. However thats not the case in many flapping wing applications.

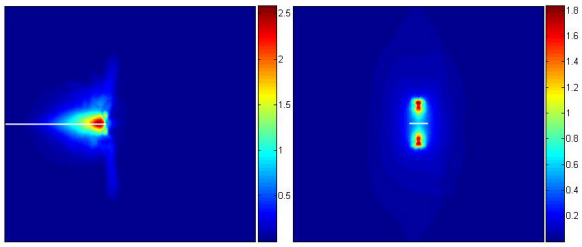

Figure 14: Mean velocity interpolated from 3D numerical data. Left: symmetry plane. Right: beam-cross section 25 mm away from tip. The flapping plate is marked as a white line.

The results for the 3D case highlight the complicated flow which is dominated by large-scale vortices that provide intensive mixing which cause a rapid divergence of the flow (Fig. 13). This is consistent with the experimental observations in this work. The 2D formulation is unable to provide an adequate simulation of the jet formation as obtained in the experimental results. For the 3D model more cycles have to be calculated to achieve a fully developed flow regime that is suitable for averaging out in planes further away from the flapping plate.

4. CONCLUSIONS

The unsteady flow induced by a piezoelectric flapping plate was experimentally investigated. A high speed PIV system was used to obtain measurements to quantify the transient behavior for the comparison with 2D and 3D LES models. The PIV measurements uncovered that the evolution of the vortices for 3D flapping wing would be much more complicated compared with those for 2D flapping wings. The 2D LES model is not able to accurately predict the flow field induced by a flapping plate with a finite span. It is planned as a future work to apply optimization algorithms on the 3D LES computational models of the vibrating plate to reduce the number of iterations to obtain a desired aerodynamic characteristic.

ACKNOWLEDGMENTS

The authors gratefully acknowledge support by the IWT (Institute for the Promotion of Innovation by Science and Technology in Flanders).

REFERENCES

[1] Toda, M. (1979) Theory of flow generation by a resonant type PVF2 bimorph cantilever vibrator. *Journal of Ferroelectrics*, Vol. 22, 911–918.

[2] Acikalin T., Wait S. M., Garimella S.V. (2004) Experimental investigation of the thermal performance of piezoelectric fans. *Journal of Heat transfer Eng.*, Vol. 25(1), 4-14.

[3] Burmann P., Raman A., Garimella S.V. (2003) Dynamics and topology optimization of piezoelectric fans. *IEEE Transaction on components and packaging technologies*, Vol. 25(4), 592–600.

[4] Cox A., Monopoli D., Cveticanin D. (2002) The development of elastodynamic components for piezoelectrically actuated flapping micro air vehicles. *Journal of Systems and Structures*, Vol. 13, 611-615.

[5] Park H. C., Kim K. J., Less S., Lee S. Y. Biomimetic flapping devices powered by artificial muscle actuators. *Proc. of UKC 2004 US-Korea Conference on Science, Technology and Entrepreneurship*, August, 2004.

[6] Chung H. C., Kummari K. L., Croucher S. L., Lawson N. J., Guo S., Whatmore R.W. Huang Z. (2009) Development of piezoelectric fans for flapping wing application. *Journal of Sensors and Actuators*, Vol. 149 A, 136-142.

[7] Acikalin B., Iverson B. D. (2005) Computational study of convection with moving wall boundary in an enclosure. *PhD Thesis*, Department of Mechanical Engineering, Purdue University.

[8] Hu H., Clemons L., Igarashi H. (2011) An experimental study of the unsteady vortex structures in the wake of a root-fixed flapping wing. *Journal of Experiments in Fluids*

[9] Kim Y. H., Cierpka C., Wereley S. T. (2011) Flow field around a vibrating cantilever: coherent structure eduction by continuous wavelet transform and proper orthogonal decomposition. *Journal of Experiments in Fluids*

[10] MIDE Technology, www.mide.com

[11] Bidakhvidi, M. A. (2009) The design of a piezoelectric fan system for the flapping wing mircro-air-vehicle application *Msc Thesis*, Department of Mechanical Engineering, Vrije Universiteit Brussel.

[12] PIVview 2C, PIVTEC GmbH